International Communications in Heat and Mass Transfer 170 (2026) 110009

Contents lists available at ScienceDirect

International Communications in Heat and Mass Transfer

journal homepage: www.elsevier.com/locate/ichmt

Experimental investigation of thermal performance of NanoEncapsulated-PCM emulsions in parallel plate thermal energy storage system

Hüseyin Kaya [a,c], Emre Alp [b], Safa Sabet [c], Bernardo Buonomo [c], Laura Fedele [d], Stefano Rossi [d], Oronzio Manca [c,*]

[a] Department of Mechanical Engineering, Bartın University, Bartın 74110, Türkiye
[b] Department of Metallurgical and Material Engineering, Bartın University, Bartın 74110, Türkiye
[c] Department of Engineering, Università degli Studi della Campania "Luigi Vanvitelli", Aversa (CE) 81031, Italy
[d] Construction Technologies Institute, National Research Council (CNR ITC), Padova (PD) 35127, Italy

ARTICLE INFO

Keywords:
NanoPCM emulsion
Thermal energy storage
Iron oxide PCM

ABSTRACT

This study investigates the thermal performance of nanoPCM emulsions (nanoPCMEs) as working fluids in parallel plate thermal energy storage system, comparing two configurations: solid aluminum walls and aluminum profile walls filled with PCM + metal foam. Three distinct nanoPCM emulsions were evaluated against pure water as a base fluid. The experimental results demonstrated superior convection heat transfer performance for all nanoPCMEs compared to pure water. In the solid aluminum wall configuration, maximum thermal energy storage reached approximately 900 kJ, with 2.0 wt% nanoPCME achieving this level twice as fast as pure water. The PCM + metal foam configuration exhibited enhanced performance, storing up to 2250 kJ of thermal energy due to PCM's high latent heat, reaching maximum storage 1.6 times faster than pure water. Notable improvements in heat transfer were observed, with nanoPCME achieving the highest average Nusselt numbers across all configurations. Maximum enhancements in Nusselt number were 34.5 % and 41.9 % for solid wall and PCM + metal foam configurations, respectively, using 2.0 wt% nanoPCME. These findings demonstrate the significant potential of nanoPCMEs for improving thermal energy storage systems and thermal control applications.

1. Introduction

Phase change materials (PCMs) are recognized for their high thermal energy storage capabilities, making them essential for enhancing energy efficiency in various applications. However, a significant limitation arises from the low thermal conductivity of many PCMs, which hampers their effectiveness in scenarios requiring rapid energy discharge [1]. This challenge has prompted researchers to explore innovative solutions, particularly through advancements in nanotechnology. The introduction of nanofluids—created by suspending nanoparticles of less than 100 nm in traditional heat transfer fluids like water, oil, and ethylene glycol—has shown promise in improving the thermophysical properties of these fluids, thus enhancing heat transfer characteristics. Recent studies have proposed the development of NanoPCM structures, which involve dispersing highly conductive nanoparticles within PCMs to address the low thermal conductivity associated with conventional PCMs [2–4]. One effective method for integrating PCMs into thermal systems is through the creation of phase-changing material mixtures. These mixtures consist of a carrier fluid with excellent transport properties combined with a PCM that exhibits high latent heat. Such systems facilitate direct thermal energy exchange between the PCM and the heat transfer fluid, leveraging large surface-to-volume ratios for efficient energy transfer [5]. Moreover, the behavior of NanoPCM emulsions (NanoPCMEs) has garnered attention for their ability to combine the latent heat storage capabilities of PCMs with the unique properties of nano-additives. Research indicates that incorporating nanoparticles can significantly enhance the heat transfer characteristics of PCM slurries, leading to improved effective heat capacity and increased thermal energy absorption without substantial temperature fluctuations [2]. The efficiency of NanoPCMEs, however, is contingent upon various factors, including the type and concentration of nanomaterials, which ultimately influence the phase change temperature and thermophysical properties of the emulsions [6].

* Corresponding author.
E-mail address: oronzio.manca@unicampania.it (O. Manca).

https://doi.org/10.1016/j.icheatmasstransfer.2025.110009

0735-1933/© 2025 The Authors. Published by Elsevier Ltd. This is an open access article under the CC BY license (http://creativecommons.org/licenses/by/4.0/).

Nomenclature

C_p	Specific heat, J/kg K
h	Convection heat transfer coefficient, W/m^2K
k	Thermal conductivity, W/mK
D_h	Hydraulic diameter, m
Nu_{avg}	Average Nusselt number
PCM	Phase change material
NanoPCME	Nanoencapsulated PCM emulsion
q	Heat flux, W/m^2
Re	Reynolds number
$\dot{V}$	Volume flow rate, L/min
t	Time, s
A_w	Heat transfer area, m^2
Q_{tot}	Total energy storage, J
T	Temperature, K
T_i	Inlet temperature, K
T_o	Outlet temperature, K
μ	Dynamic viscosity, Pa-s
ρ	Density, kg/m^3

The addition of metal oxides and nucleating agents not only bolsters the thermal conductivity of NanoPCM emulsions but also contributes to the stability of these nanofluids under operational conditions, mitigating issues such as sedimentation and ensuring consistent performance over time [7]. Investigations into the flow characteristics and thermal behavior of water-based NanoPCM emulsions in microchannel systems have revealed that optimal configurations can enhance heat transfer while effectively managing the inherent fluid dynamics [8]. The implications of these advancements are far-reaching, with potential applications spanning electronic cooling, energy-efficient buildings, and concentrated solar power systems [9]. By harnessing the latent heat associated with phase change processes, NanoPCMEs can effectively mitigate temperature fluctuations and improve the overall efficiency of thermal energy management systems [10]. This innovative approach positions NanoPCMEs as viable candidates for next-generation thermal energy storage systems, promoting a more sustainable and effective utilization of thermal energy resources [11].

In recent years, the utilization of nanoPCMs in heat transfer and thermal energy storage systems has attracted considerable attention due to their enhanced efficiency. Comprising PCMs combined with nanoparticles, nanoPCMs exhibit improved thermal properties, including increased thermal conductivity and reduced supercooling, making them suitable for diverse applications, from industrial processes to building temperature regulation [9,12,13]. For instance, Singh et al. conducted an experimental study on nanoPCM structures formed by dispersing CuO and Al_2O_3 nanoparticles in a sugar alcohol PCM, highlighting their potential in solar energy storage systems [14]. Similarly, Kok determined that varying fin geometries could significantly affect melting characteristics, reducing melting time by up to 63 % [15]. Nóbrega et al. investigated the energy storage properties of nanoPCM structures, finding a 47 % increase in solidification phase completion with a 10 % Al_2O_3 concentration in finned structures [16].

Further research by Kabeel et al. demonstrated the effectiveness of nanoPCMs prepared with graphene oxide nanoparticles in solar distillation systems, revealing a 52 % increase in thermal conductivity compared to conventional PCMs [17]. Sathishkumar et al. explored the thermal performance of low-capacity energy storage systems using graphene nanoparticles, achieving reductions in charging and discharging times by up to 22.8 % [18]. Kalbande et al. conducted an analytical study on a hybrid thermal energy storage system, finding that nanoPCM outperformed pure paraffin wax in thermal conductivity and phase transition times [19].

Recent literature emphasizes the advantages of nanoPCMs in latent heat thermal energy storage (LHTES) systems. For instance, Farsani et al. illustrated that paraffin-alumina nanoPCMs effectively manage thermal energy in high-powered electronics cooling systems, optimizing thermal performance through successive melting and solidification cycles [20]. Liu et al. addressed challenges related to instability and supercooling in PCM emulsions, paving the way for more reliable thermal energy storage solutions by optimizing formulations [21]. The thermal conductivity of nanoPCMs is crucial for their performance in heat transfer applications. Zhou et al. demonstrated that functionalized graphene oxide significantly enhances the thermal properties of PCM formulations, improving heat transfer rates during charging and discharging phases [22]. Gamot et al. further supported the notion that high internal phase emulsions with minimal graphene oxide content can exhibit remarkable thermal conductivity [23].

Stability remains a critical consideration for the practical application of nanoPCMs. Mhiri et al. explored the thermal behavior of composite materials comprising nanoPCMs and aluminum foam, revealing that such composites mitigate leakage issues during phase transitions while maintaining structural integrity and thermal performance [24]. This stability is vital for ensuring the longevity and reliability of thermal energy storage systems, especially in dynamic environments with fluctuating temperatures. The versatility of nanoPCMs extends beyond traditional applications, as evidenced by Liu et al.'s work on micro-encapsulated PCMs for various uses, including textiles and construction materials [25]. This adaptability underscores the significance of nanoPCMs in advancing thermal energy storage technologies. Despite the growing body of research on NanoPCM emulsions as working fluids for thermal energy storage and heat transfer performance, there remains a notable gap in comprehensive analyses that integrate both iron and paraffin nanoparticles as emulsions within thermal energy systems. Addressing this gap is essential, as the incorporation of metal oxide nanoparticles can significantly enhance thermal control in applications such as electric components and solar collectors.

As can be seen from the literature, the integration of nanoPCMEs into heat transfer and thermal energy storage systems represents a promising avenue for enhancing thermal management solutions. The ongoing research into stability, thermal conductivity, and innovative design of nanoPCMs is crucial for overcoming existing challenges and unlocking their full potential in various applications. As the demand for efficient thermal energy storage solutions continues to rise, the development of advanced nanoPCM formulations will play a pivotal role in shaping the future of thermal management technologies. For these reasons, thermal performance of nanoPCMEs containing two different iron oxide nanoparticles for parallel plate heat thermal energy storage (TES) system were experimentally investigated.

2. Materials and methods

2.1. Production of NanoPCM emulsions

Studies were carried out on the preparation of nanoPCM emulsions (nanoPCMEs) mixtures and the stabilization of these structures. To prepare nanoPCMEs, nanofluid and nanoPCM syntheses were carried out. Two different iron oxide nanofluids were prepared to achieve more stable and homogeneous nanoPCM emulsions. Then, nanoPCM emulsions were prepared by using RT55 (Rubitherm) paraffin wax, which is one of the most widely used PCMs. Both preparation methods processes are detailed below.

Nano-PCM emulsions require careful concentration management to optimize thermal performance for applications in heat transfer and thermal energy storage. A concentration limit of approximately 2.0 wt% has been established based on factors such as emulsion stability, thermal properties, and processing ease. Higher nanoparticle concentrations can increase viscosity, affecting flow and stability, while excessive stabilizing agents may lead to particle flocculation and reduced effectiveness.

Studies indicate that maintaining a 2.0 wt% concentration enhances thermal conductivity and latent heat storage without compromising heat transfer efficiency [26,27]. Additionally, this concentration allows for optimal particle dispersion, promoting effective interactions between the PCM, metal oxide particles and the base fluid [28]. The decision to limit concentration also considers manufacturing challenges, as higher concentrations complicate formulation processes. Overall, a 2.0 wt% concentration is a strategic choice that balances stability, thermal management, and practical processing considerations, ensuring the reliability of these emulsions in relevant applications [29].

The nanofluid preparation involved a two-step approach, which was selected specifically because it demonstrates superior performance with metal oxide nanoparticles compared to metal particles [30]. The process began with dispersing particles in distilled water. To achieve a stable and uniform mixture, magnetic and ultrasonic mixing techniques were employed, taking into account interparticle forces. The nanoparticles were synthesized using the hydrothermal method in autoclave reactors. This method was chosen primarily for its effectiveness in creating metal oxide nanostructures. The hydrothermal approach offers several advantages: it operates at lower temperatures, uses environmentally friendly solutions, provides cost-effective production, and enables the synthesis of highly homogeneous nanoparticles with controlled size and morphology.

Two different iron oxide samples were synthesized using similar methods but distinct procedures. For the first sample a mixture was prepared by dissolving iron (II) chloride tetrahydrate (0.05 mol), sodium sulphate (0.025 mol), and urea (8.3 mmol) in 300 ml of ultrapure water with magnetic stirring. This solution was placed in an autoclave at 60 % capacity and heated to 180 °C for 12 h in a Teflon-lined stainless-steel container. The second sample used identical quantities of the same chemicals but was dissolved in 350 ml of ultrapure water instead. This mixture was sealed in the autoclave at 70 % capacity and heated to a slightly lower temperature of 160 °C, also for 12 h. Both samples underwent the same post-processing steps: they were allowed to cool naturally to room temperature inside the furnace. The resulting products were then purified through repeated centrifugation and washing cycles using ultrapure water and ethanol to remove any remaining by-product. Finally, the particles were dried overnight at 65 °C [31].

To produce nanoencapsulated-PCM, chemical dissolution and nucleation procedures (solvent-assisted) were followed, that is an innovative method and provide fast product production as schematically represented in Fig. 1. The nanoencapsulated-PCM production began with the preparation of two separate solutions: PCM dissolved in hexane and sodium dodecyl sulfate (SDS) dissolved in ultrapure water. SDS was selected as the capping agent because it proved most effective at reducing particle size and maintaining emulsion stability over extended periods, as noted in reference [32]. To achieve the most stable emulsions, a mass ratio of 1:8 (SDS to PCM) was found to be the most effective. Both solutions underwent sonication treatment for several minutes. Following this, the SDS-water solution was gradually introduced into the PCM-hexane mixture over a period of several hours. The resulting emulsions were then heated at 90 °C for 2–3 h to remove all hexane, resulting in a pure nano-encapsulated paraffin emulsion in water. Throughout the heating process, any water lost to evaporation was continuously replaced, and additional water was added as needed to achieve the target PCM concentration.

These two water-based dispersions were characterized individually and were created by the planned specific mixture structure to determine their thermophysical properties. This new nanofluid-NanoPCM dispersion obtained was subjected to ultrasonic and magnetic stirring process to provide a stable and homogeneous fluid. In this method, using SDS water and chemical dissolution of paraffin in hexane, nucleation is aimed at obtaining spherical-like particles. SDS surfactant was used for stable NanoPCM dispersion which has provided the coated spherical like PCM nanoparticles and the new dispersion was obtained by nucleation [33]. Fig. 2 gives the sample steps of NanoPCME preparations.

Furthermore, the NanoPCM emulsions were experimentally analyzed with two different iron oxide nanoparticles for two main reasons. Firstly, to decrease the subcooling effect by serving as a nucleating agent. Secondly, to alter the optical characteristics of nano-emulsion, resulting in the creation of a high thermal conductivity working fluid.

This solvent assisted technique produced nanofluid-nanoPCM mixture dispersions that were stable and homogenous. The total nanoparticle weight percentage of each dispersion is 2.0 wt%. These two mixture dispersions contain nanoPCMs and different metal oxide nanoparticles that were used for heat transfer and heat accumulation experiments in forced convection flow.

Particle size analysis and melting-solidification characteristics of nanoPCMEs produced using the solvent-assisted production method were examined. Hexane was used as the solvent and SDS was used as the agent, and homogeneous dispersions were obtained. Figs. 1 and 2 give the preparation procedure and samples of nanoPCMEs. The abbreviations of working fluids in this paper are: NanoRT55 (nanoPCME_1), NanoRT55 + iron oxide I (nanoPCME_2) and nanoRT55 + iron oxide II (nanoPCME_3).

2.2. Characterization of NanoPCMEs

The microstructural characteristics of synthesized nanoparticles and nanoPCMs were carried out using a field emission gun scanning electron microscope (TESCAN™ MAIA XMU). Typical low and high-magnification Scanning Electron Microscopy (SEM) images of the

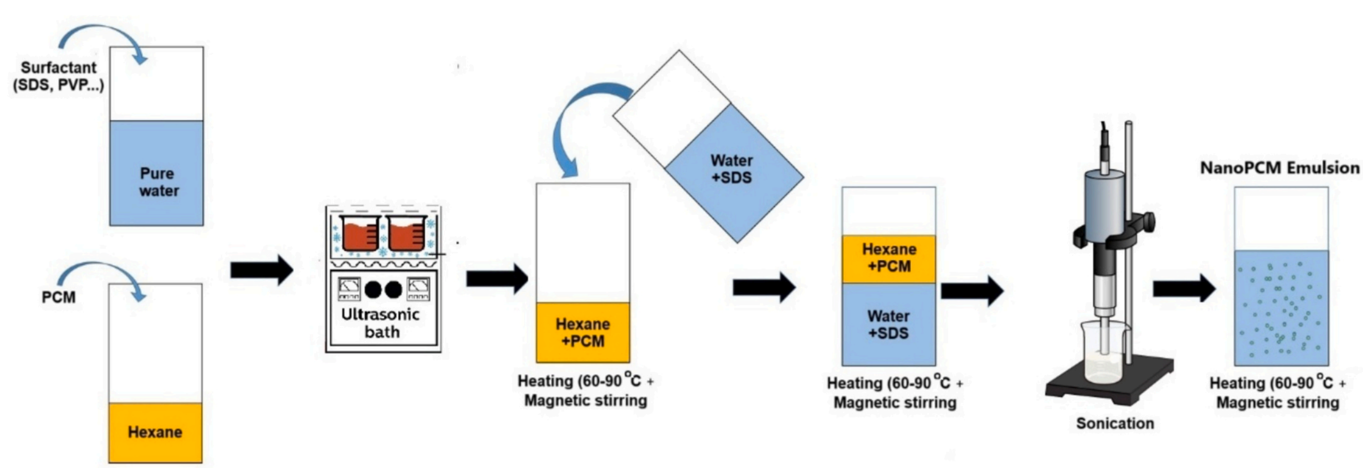

Fig. 1. Procedure of Solvent Assisted NanoPCM Emulsion preparation.

Fig. 2. Preparation procedure and samples of nanoPCMEs.

produced nanoparticles are given in Fig. 3 with images belonging to nanoPCME_1, and spherical like iron oxide I (IO1) and iron oxide II (IO2). The micrograph images of low and high-magnification scanning electron microscopy FESEM images belong to as-synthesized produced nanoparticles. As seen from the images, they are in different morphologies and sizes from each other. Furthermore, all nanoparticles produced are formations of uniform and monodisperse within themselves. Although synthesize of nanoPCMs is quite challenging, nearly homogenous dispersions were obtained. Fig. 3a gives the nanoPCME containing only RT55. Nanoparticles in Fig. 3b and c refer to two different iron oxide nanoparticles, IO1 and IO2 respectively. They have spherical morphology and average 140 nm particle size for IO1 and 170 nm for IO2. Other dispersions were also prepared using metal oxide nanoparticles and nanoPCM particles at different concentrations to be used in experiments. Encapsulated NanoRT55 paraffin nanoparticles were prepared and dispersed with different nanofluids by using an ultrasonicator. SEM images of nanoPCMs (encapsulated RT55 particles) are shown in Fig. 3a, and it is seen that a structure close to homogeneous distribution is obtained. Spherical like particle morphologies were obtained. These two dispersions (nanofluid-nanoPCMs) were physically mixed, and then a stable homogeneous NanoPCMEs dispersion was obtained by sonicating for another 10 min with the ultrasonic bath (Hielscher UP400S) given in Fig. 2.

X-ray diffraction (XRD) analysis was performed to determine the phase composition of the synthesized particles. The diffraction patterns, presented in Fig. 4, show that all observed peaks match the JCPDS file data (JCPDS card no. 33–0664), confirming a trigonal hematite (α-Fe_2O_3) crystal structure with space group R-3c and lattice parameters a = b = 0.503 nm and c = 1.373 nm. While IO1 samples exhibited pure hematite phase, IO2 samples contained a mixture of trigonal hematite crystal structure and a minor phase of orthorhombic goethite crystal structure (FeO(OH)). The XRD pattern of IO1 displayed sharper and

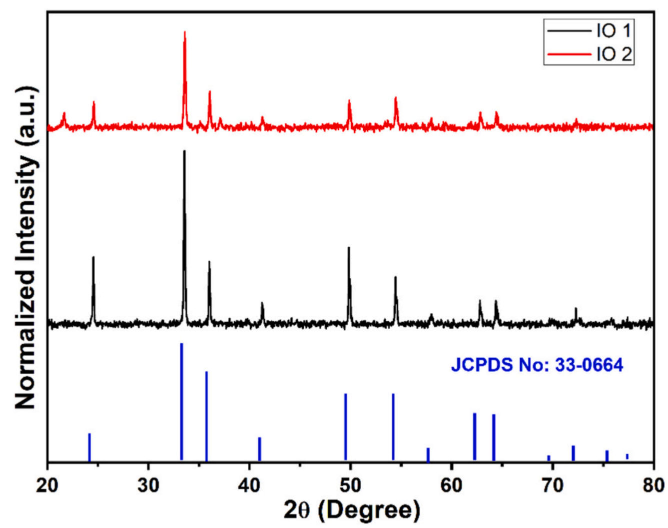

Fig. 4. XRD patterns of hydrothermally synthesized iron oxide nanoparticles.

more intense diffraction peaks compared to IO2, indicating higher crystallinity in the IO1 sample.

The average particle size of all mixture dispersions is presented in Fig. 5. NanoPCME_1, which contains only RT55 encapsulated nanoparticles used in the experiments, has an average particle diameter of 105 nm and that result meets quality criteria. The average particle size of nanoPCME_2 was determined as approximately 142 nm. Also, the average particle diameter of nanoPCME_3 was obtained as 170 nm, and there was a bit different from the other dispersions. In these results, the distribution of nanoparticles was obtained between 158 nm – 170 nm

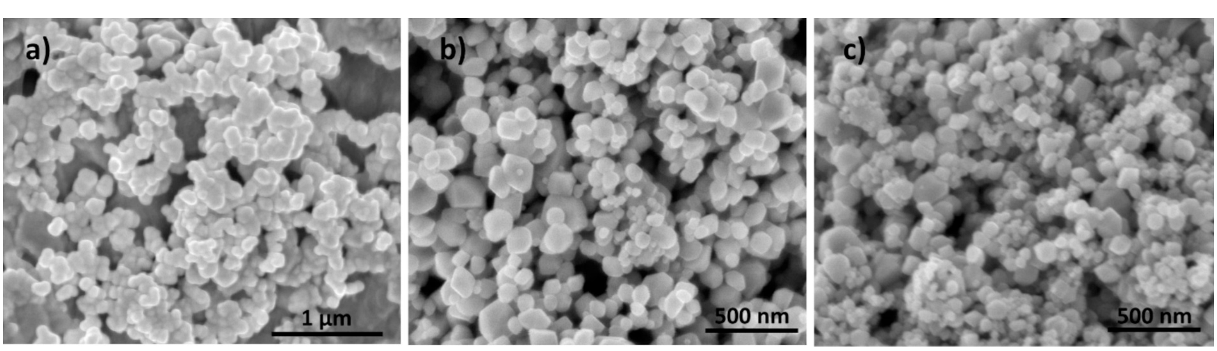

Fig. 3. SEM images of (a) NanoEncapsulated-PCM, (b) Iron oxide I nanoparticles and (c) Iron oxide II nanoparticles.

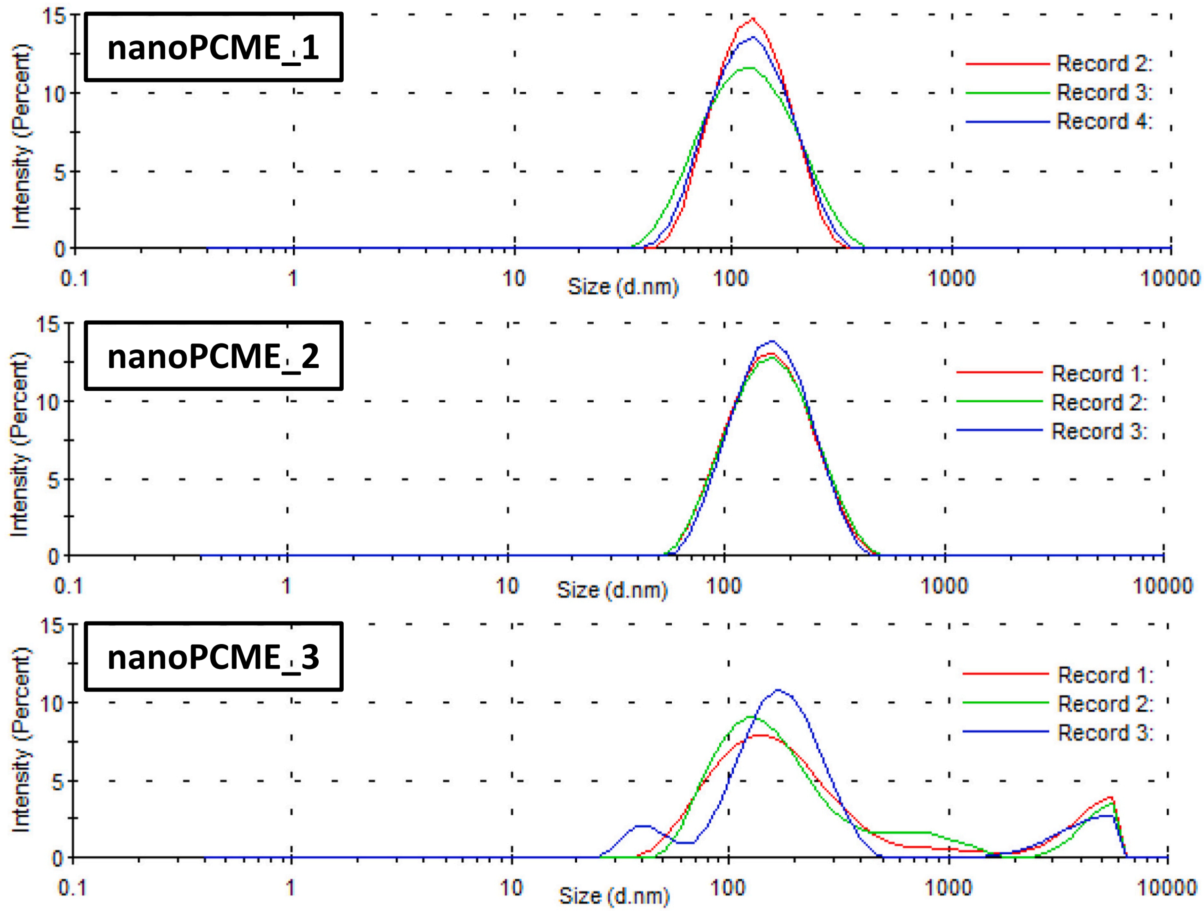

Fig. 5. Particle distribution and average particle size analysis of each NanoPCME.

with three measurements with the ratio of 84.4 %, 79.1 % and 77.7 %, respectively. Despite these results of NanoPCME_3, since the particle distribution obtained is high, it can be accepted that the results are valid for the specified particle sizes.

Phase change behavior analyses were carried out by means of heating and cooling. The differential scanning calorimetry (DSC) results for the nanoPCM emulsions reveal significant insights into their melting and solidification behaviors in Fig. 6. In the first graph, a pronounced endothermic peak is observed around 53.8 °C, indicating the melting

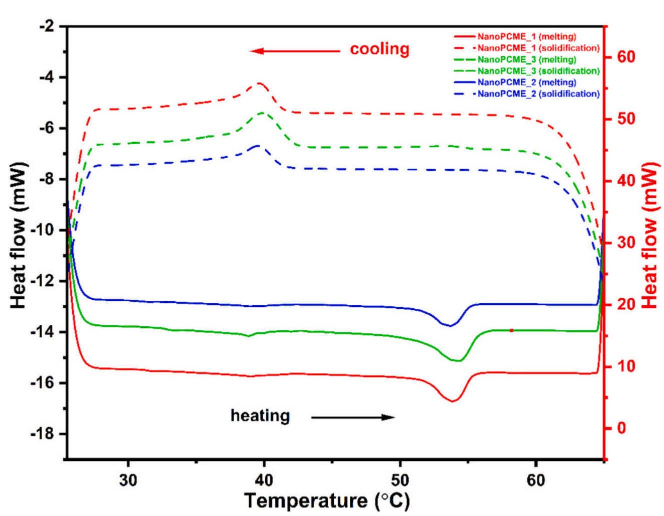

Fig. 6. DSC results of all NanoPCMEs.

transition of the nanoPCM. This suggests that emulsion effectively absorbs heat, which is crucial for applications in thermal energy storage. Conversely, the second graph displays an exothermic peak at 39.6 °C, corresponding to the solidification process. This dual behavior highlights the phase change capabilities of the nanoPCM emulsions, making them suitable for applications where thermal regulation is essential. Since the PCM particles are encapsulated with SDS the difference of solidification and melting peaks are more pronounced. The sharp transitions observed in both melting and solidification phases suggest a well-defined phase change, which is beneficial for optimizing thermal management systems. When comparing nanoPCME_2 and nanoPCME_3, it can be seen that the peak resulting from the presence of IO nanoparticles in nanoPCME is lower. This indicates that sub-cooling has been reduced. The area between the solidification and melting peaks of nanoPCME_2 is larger than the bulk PCM since the nanoencapsulation of PCM particles in deionized water provides more latent heat.

2.3. Experimental procedure

In order to test thermal energy storage and heat transfer performance of the nanoPCMEs a forced convection flow experimental setup was used. Water based NanoPCMEs containing spherical like RT55 and Fe_2O_3 nanoparticles were tested. A test section was prepared with aluminum parallel plates like a mini channel at first for the experimental analysis. Aluminum plates were used due to the high thermal conductivity. Experiments were conducted at laminar flow conditions (*Re* ⟨2000). All experiments were carried out with three different volume flow rates tested as 0.55 L/min, 0.87 L/min and 1.1 L/min that were adjusted with the peristaltic pump and by using a differential pressure flow meter. Temperature measurements were taken using J-type thermocouples with a sensitivity of ±0.1 °C. Constant temperature water bath was used to calibrate the thermocouples. The calibration procedure was conducted by using constant temperature thermal bath by increasing temperature from 30 °C to 70 °C with 5 °C increment. A thermostatic bath was used to apply constant inlet temperature. The inlet temperature was fixed at 63 °C during the experiments. Also, the initial temperature was set at 25 °C for all experiments. Two different structures of experimental test sections (aluminum heat exchangers) were used in the experimental setup. All in all, three different flow rates were used for each working fluid and parallel plate heat exchanger configurations. Also, four different configurations come from the different weight concentrations (pure water, 0.5 %, 1.0 % and 2.0 %). That means 24 independent experiments were performed by considering all variables. Three repeated experiments were performed for all conditions to eliminate the error deviations. The properties of the materials are presented in Table 1.

The integration of nano-dispersed working fluids in heat exchangers represents a significant advancement in the field of thermal management, enhancing both heat transfer efficiency and thermal energy storage capabilities. NanoPCMEs, which are engineered by suspending nanoparticles in conventional heat transfer fluids, exhibit improved thermal conductivity and heat transfer characteristics compared to their base fluids. This discussion will address the principles of heat transfer and thermal energy storage in heat exchangers using nano-dispersed working fluids and examine how these innovative materials can optimize performance, reduce energy consumption and contribute to more sustainable thermal systems. By analyzing the mechanisms at play and the implications for various applications, we can better understand the transformative potential of nanotechnology in thermal energy management. The results of parallel plate heat exchanger with metal foam embedded walls are presented and discussed.

Fig. 7 combines a photo of the parallel plate test section and the scheme of the whole experimental setup. Solid aluminum plates having 20 mm thickness were used to establish the 20 mm plate channel to get the results for the base case by using pure water. After that this test section was integrated into the experimental setup as seen in that figure. In this case the aim is to investigate the thermal energy storage of the parallel plates. Thermocouples were placed to measure the inlet, outlet, and the wall temperatures. It was decided to use hot fluid inlet boundary condition at 63 °C to test heat accumulation. Since experiments with PCM and nanoPCMEs were considered, it is better to use an inlet temperature higher than the melting points of the used paraffin PCMs. The inlet temperature of the water was arranged to be constant by using a thermostatic water bath. After the pump had been operated, the temperature measurements were taken from the inlet, outlet and through the wall. Since it is a time dependent experiment, it is necessary to observe the temperature variation with respect to the time. 3-D printed lofted parts were inserted into the inlet and outlet of the rectangular channels to fit them to the experimental setup. High temperature resistant silicon adhesives were used.

The channel used in the setup has two different configurations. One

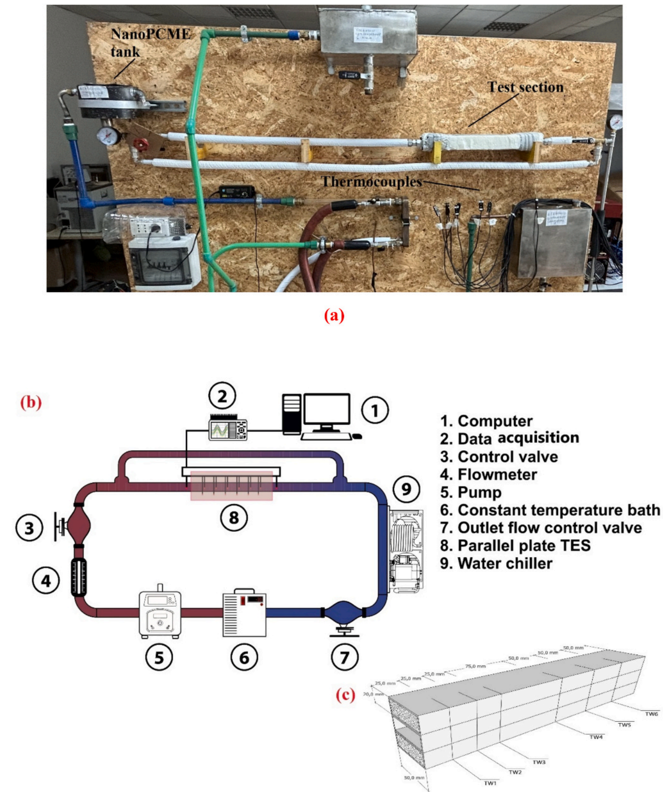

Fig. 7. Experimental setup: (a) photo of the complete experimental setup, (b) scheme of the experimental setup and (c) sketch of the test section.

configuration consists of two aluminum parallel plates with a thickness of 20 mm each. The other configuration has the channel walls made up with aluminum rectangular hollow section filled with open metal foam and phase change material, as shown in Fig. 8a. The open metal foam is of aluminum with a porosity equal to 0.949 and a pore density of 20 PPI (pore per inch), Fig. 8b. The phase change material is RT55. The properties of the materials are presented in Table 1. In both the configurations, the gap between the two plates is equal to 20 mm in all tests.

2.4. Data reduction

During the test, all temperature data are tracked using a data acquisition unit. All experiments were conducted as time dependent. The convective heat transfer coefficient of working fluid inside the parallel plate heat exchanger can be calculated based on Newton's

(a) (b)

Fig. 8. Composite wall for the second configuration: (a) aluminum rectangular hollow section with metal foam and PCM, and (b) open cell aluminum foam used in the walls.

Table 1
Properties of RT55, Fe_2O_3 and water [34,35].

Properties	RT-55 Rubitherm	Fe_2O_3	Water (60 °C)
Density (kg/m^3)	–	5240	977
Density in solid state, ρ_s (kg/m^3)	880	–	–
Density in liquid state ρ_l (kg/m^3)	770	–	–
Specific heat capacity, C_P (J/kg K)	2000	628	4190
Thermal conductivity, k (W/m K)	0.2	12.55	0.663
Dynamic viscosity, μ (kg/m.s)	0.0235	–	0.000404
Thermal expansion coefficient, β (1/K)	0.0001	7×10^{-6}	–
Latent heat, (J/kg)	170,000	–	–
Melting temperature, T_l (°C)	57	–	–
Solid temperature, T_s (°C)	51	–	–

cooling formula using Eq. (1) [35].

$$h = \frac{Q_{tot}}{A_w(T_w - T_b)} \quad (1)$$

where Q is the heat transfer rate coming from the heat transfer fluid. Bulk temperature was calculated by using the inlet and outlet temperature at specified time by using Eq. (2) [35].

$$T_b = \sum_0^t \frac{T_i - T_o}{2} \quad (2)$$

Total heat energy stored by the system for aluminum solid walls and PCM + metal foam walls can be calculated with Eq. (3) and Eq. (4) [7,18].

$$Q_{tot} = \sum_0^t mc_{p,f}(T_i - T_o)_t \quad (3)$$

$$Q_{tot} = \sum_0^t m\left[c_{p,s}(T_m - T_i) + LH_f + c_{p,l}(T_e - T_m)\right] \quad (4)$$

where T_m is melting temperature and T_e is equilibrium temperature. LH_f is the latent heat capacity of phase change of the RT55 PCM.

Average wall temperature values were calculated by using Eq. (5) with six thermocouples at the walls as follows [6,7]:

$$T_w = \frac{1}{6}\sum_{i=1}^{6}\left(T_{w,i} - \left(\frac{z_1 q_{flux}}{k_{Al}} + \frac{z_2 q_{flux}}{k_{PCM}}\right)\right) \quad (5)$$

where, $T_{w,i}$ is the temperature of wall denoted by each thermocouple, z_1 and z_2 are the vertical distances from channel surface to the thermocouple location which are 3 mm and 17 mm respectively, k_{Al} is the thermal conductivity of aluminum channel (205 W/m K), q_{flux} is the heat flux coming from the hot working fluid.

Experiments were carried out in laminar flow conditions according to the corresponding Reynolds number of the flow which was calculated by using Eq. (6) [35].

$$\mathrm{Re} = \frac{4\rho\dot{V}}{\pi D_h \mu} \quad (6)$$

where $\dot{V}$is the volume flow rate of the working fluids. According to measurements during the experimental studies Nusselt number values and distributions were obtained by using Eq. (7) [35].

$$Nu = \frac{hD_h}{k_{htf}} \quad (7)$$

where the subscript 'htf' refers to the heat transfer fluid.

2.5. Uncertainty analysis

Uncertainty analysis serves as a crucial indicator of data accuracy and the proper utilization of measurement devices in experimental studies. Furthermore, it is also important in terms of repeatability. To assess the sensitivity of the results, an uncertainty analysis was performed based on the measurements obtained during this investigation. The dimensionless numbers used to determine the flow parameters are the *Re* and *Nu* numbers. When the formulas of them are examined, the parameters measured during the experiments are the flow rate, wall, inlet and outlet temperatures. The error estimation was performed according to uncertainty calculation procedure of each independent variable. The uncertainty values of these parameters were used to calculate the uncertainty amounts for the *Nu* number and energy stored, eventually the overall uncertainty. The average uncertainties associated with the Nusselt number (*Nu*) and stored energy were determined to be 2.6 % and 2.7 %, respectively. Consequently, the overall uncertainty for the experiments was calculated to be 5.3 %.

Table 2 presents the uncertainty values for each component analyzed. The Root Sum Square (RSS) method, recognized as a widely accepted and reliable approach, was employed to conduct uncertainty analysis for these parameters. Eq. 8 describes the degree of uncertainty for each parameter observed in the experiment as previously outlined in the literature [36].

$$\frac{\partial w}{w} = \left[\sum_{i=1}^{N}\left(\frac{\partial x_i}{x_i}\right)^2\right]^{1/2} \quad (8)$$

Where N indicates the number of measurements and x_i denotes the independent parameter.

The parameters processed from the data, including inlet and outlet temperatures, average wall temperature, Nusselt number, energy stored are presented along with their relative errors. The error analysis indicates that the temperature difference between the inlet and outlet is very small when the flow reached thermal equilibrium or the flow rate is high. Since the actual heat transfer is based on the temperature difference between the inlet and outlet, an increase in flow rate boosts this error, leading to a corresponding increase in the errors associated with wall temperature calculations. Additionally, geometric errors, attributed to manufacturing inaccuracies and human operational errors.

3. Results and discussions

The study examines thermal performance of a parallel plate heat TES, highlighting how the flow rate and the concentration of nanoPCME influence both the Nusselt number and the thermal energy storage capacity. There are two different configurations: one is parallel plate TES with solid aluminum walls the other is a parallel plate TES with aluminum plates filled with PCM embedded in metal foams. The findings reveal that variations in flow rate significantly influence the heat transfer efficiency, as evidenced by changes in the Nusselt number. Additionally, the concentration of nanoPCME plays a crucial role in enhancing thermal energy storage, demonstrating improved heat transfer characteristics at optimal concentrations. The results will be analyzed in relation to the research questions posed at the outset, highlighting key trends, patterns, and anomalies observed during the experimentation. By integrating those results with relevant literature, we seek to offer a detailed insight into the subject and propose directions for future studies.

3.1. Effects of flow rate, NanoPCME concentration and heat exchanger configuration on Nusselt Number

Fig. 9 illustrates the relationship between the Nusselt number and two different experimental parameters: flow rate and concentration of nanoPCME_1 in the solid walled parallel plate heat exchanger. Figures were created with error bars by using calculated maximum error rates for each parameter as 2.6 %. In Fig. 9a, which focuses on varying

Table 2
Uncertainty of each measuring apparatus.

Item	Range	Error
Input		
Length of flow channel (mm)	300 mm	± 2 mm
Hydraulic diamater (mm)	24.9 mm	± 0.1 mm
NanoPCME weight fraction (%)	0–2.0	± 0.001 %
Measured		
Volume flow rate (L/min)	0.55–1.1	± 0.5 %
Wall temperature (°C)	25–63	± 0.97 %
Temperature difference (ΔT) (°C)	0.45–9.4	± 0.62 %
Result		
Nusselt number	3.8–16.7	± 2.0 % - 2.6 %
Energy stored (kJ)	0.326–2245	± 2.1 % - 2.7 %

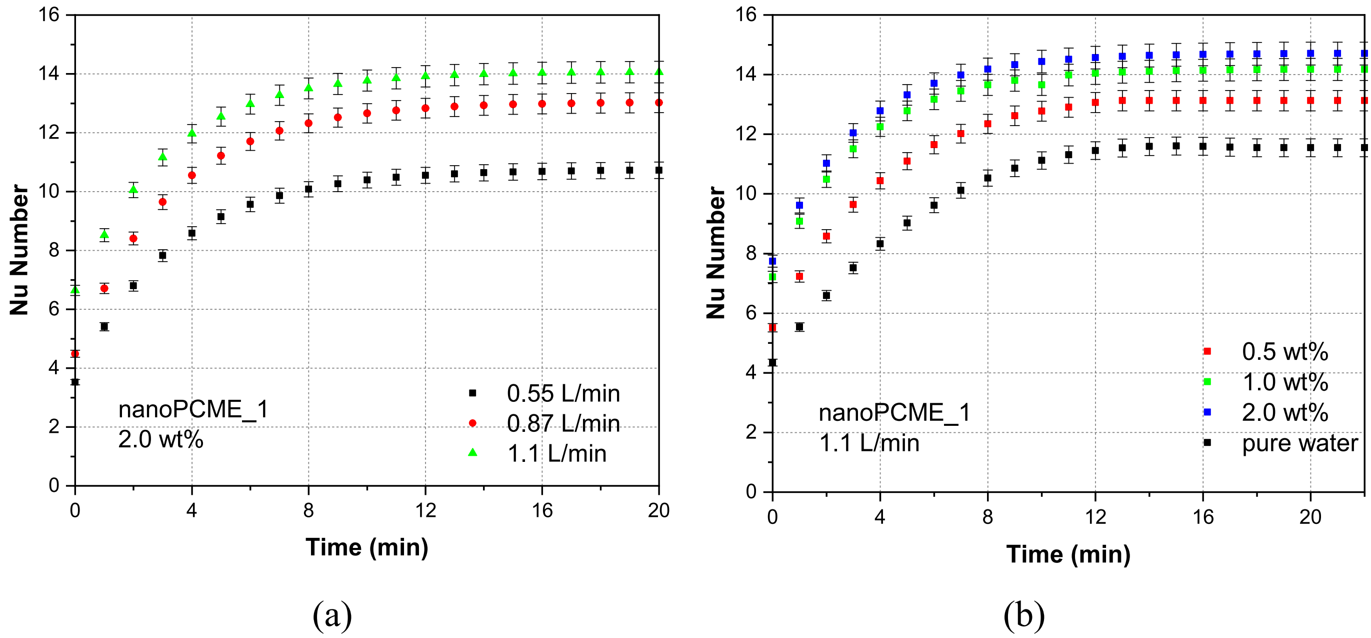

Fig. 9. Nusselt number change for nanoPCME_1 according to flow rate and concentration.

flow rates (0.55 L/min, 0.87 L/min, and 1.1 L/min) with a fixed concentration of 2.0 wt%, it was obtained that as the flow rate increases, the Nusselt number shows improvements. This trend can be attributed to the enhanced convective heat transfer associated with higher flow velocities, which promotes better mixing and reduces thermal boundary layer thickness. The increase in Nusselt number appears to be significant, particularly between the lower flow rates, indicating a strong dependency on flow conditions. The enhancement of Nusselt number with volume flow rate was obtained as 19.7 %. In Fig. 9b, the concentration of nanoPCME_1 varies (0.5 wt%, 1.0 wt%, and 2.0 wt%) while keeping the flow rate constant at 1.1 L/min. The Nusselt number also increases with higher concentrations of nanoPCME_1. This suggests that the presence of nanoparticles enhances the thermal conductivity of the fluid, leading to improved heat transfer performance. The rate of increase in the Nusselt number with concentration is notable, particularly from 0.5 wt% to 1.0 wt%, indicating that even modest increases in nanoparticle concentration can significantly impact heat transfer efficiency. The maximum Nusselt number improvement with 2.0 wt% nanoPCME_1 is 27.3 %. Together, these graphs highlight the critical roles that both flow rate and concentration play in optimizing thermal performance in nanofluid applications. On the other hand, the increase in the concentration of nanoPCMEs typically leads to an increase in viscosity, which in turn affects pumping power. Viscosity of nano emulsions typically increases non-linearly with the concentration of nanoparticles. As viscosity increases, the total dynamic head required by pumps rises, leading to lower flow rates and decreased efficiency in thermal exchanges [37]. Higher energy pumping requirements can lead to increased operational expenses over time, particularly in industrial applications where continuous operation is needed. Consequently, appropriate control of nanoPCM concentration is critical to blend thermal performance with economic feasibility, focusing on maintaining viscosity levels that can optimize both pumping efficiency and thermal performance

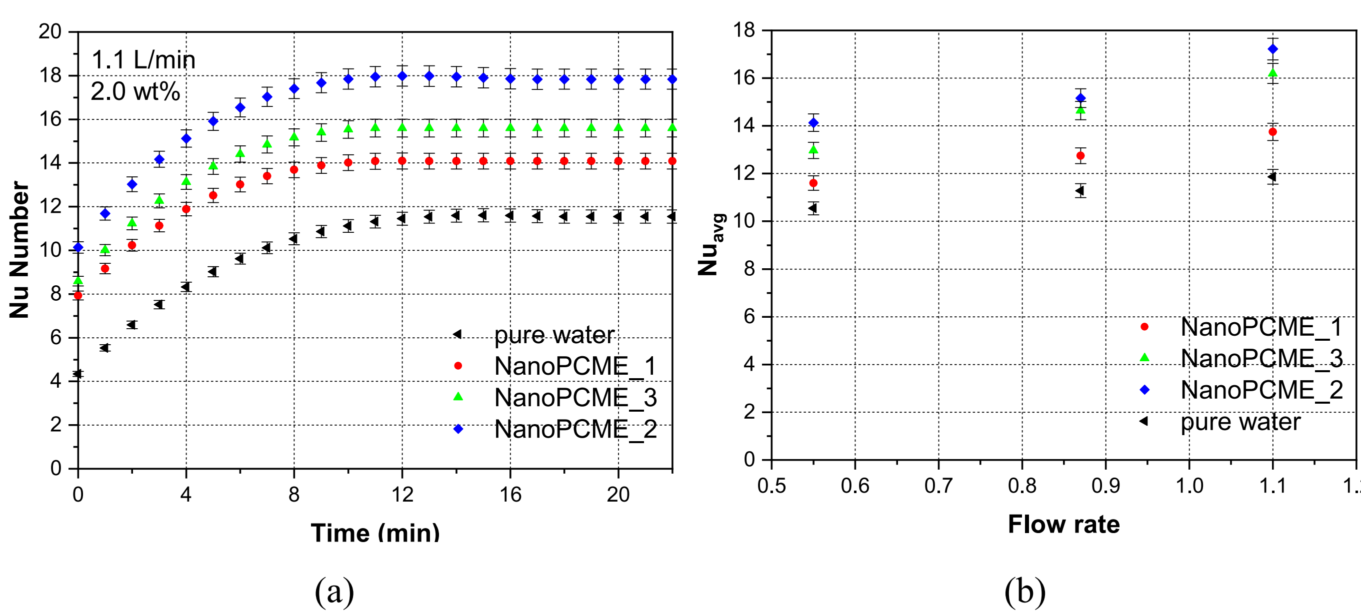

Fig. 10. (a) Nusselt number variation for different nanoPCME at 1.1 L/min flow rate and 2.0 wt% and (b) Average Nusselt number values.

[37,38].

Fig. 10 shows the relationship between the Nusselt number and both time and flow rate for various nanofluid compositions at a concentration of 2.0 wt% and average Nusselt numbers for different nanoPCME. In Fig. 10a, which plots *Nu* over time at a constant flow rate of 1.1 L/min, it is observed that the Nusselt numbers for different nanofluids increase steadily. For instance, NanoPCME_1 shows a gradual increase, while the combinations of ferro nanoparticles with nanoRT55 particles exhibit higher *Nu* values, indicating enhanced thermal performance. This trend suggests that the addition of nanoparticles significantly improves heat transfer properties, with an approximate increase in Nusselt number of around 0.2 to 0.5 per minute for these mixtures. In Fig. 10b, which depicts average *Nu* values against varying flow rates, a clear trend emerges as the flow rate increases from 0.5 to 1.1 L/min, the Nusselt numbers also rise as previously reported in [6,7]. The data points show that NanoPCME_1 has lower average *Nu* values compared to the nanoparticle mixtures, which reflects their lower heat transfer efficiency. The increase in *Nu* with flow rate suggests that higher velocities enhance convective heat transfer, leading to improved thermal conductivity. Overall, the analysis indicates a positive correlation between both flow rate and nanoparticle concentration on the Nusselt number, reinforcing the importance of these factors in optimizing thermal performance in nanofluids.

Fig. 11 demonstrates that the NanoPCME fluids, which contain nanoparticle-enhanced PCM, have significantly higher wall temperatures compared to pure water at the same time. This indicates the NanoPCME fluids are able to store and release more thermal energy than pure water. This indicates efficient heat transfer from the metal foam and PCM to the working fluid. The three NanoPCME samples demonstrate a more gradual temperature increase than water with the faster melting period. The differences in thermal responses can be attributed to the varying thermophysical properties and heat transfer characteristics of the NanoPCMEs compared to pure water. The NanoPCME samples likely have higher thermal capacities and latent heat storage abilities, which result in a more moderate temperature rise as the PCM undergoes phase change. Overall, this data provides valuable insights into the thermal management capabilities of parallel plate heat exchangers with PCM-enhanced materials. The clear trends observed across the different working fluids demonstrate the importance of selecting the appropriate material composition and operating conditions to optimize system performance for applications such as thermal energy storage and management.

Fig. 12 provides valuable insights into the behavior of the Nusselt number under varying conditions, particularly focusing on different working fluids and their flow rates over time. Fig. 13a shows the evolution of the Nusselt number over time for the same working fluids at a constant flow rate of 1.1 L/min. The curves for NanoPCME_1 rise steadily over time, indicating improved thermal performance as the system stabilizes. NanoPCME and iron oxide mixtures also show gradual increases, reinforcing the idea that these nanofluids maintain their thermal efficiency over time. Meanwhile, pure water remains relatively stable, confirming that nanofluids significantly outperform water in terms of heat transfer efficiency. In summary, both graphs highlight the substantial impact of using nanoPCMEs compared to conventional fluids like water. Fig. 12b presents the relationship between the average Nusselt number and volume flow rate for various working fluids, it is observed that NanoRT55 displays distinct Nusselt numbers. The mixtures of nanoPCME with iron oxides also exhibit increased Nu_{avg} values, indicating that the addition of nanoparticles enhances thermal performance. In contrast, water, serving as a base fluid, shows the lowest Nu_{avg}, which is expected due to its lower thermal conductivity compared to the nanofluids. The inclusion of NanoPCME_2 further raises the Nu_{avg} to around 2.6, while NanoPCME_3 also contributes positively, suggesting that both iron oxide nanoparticles enhance thermal properties when combined with NanoRT55. The addition of nanoparticles not only increases the initial Nusselt number but also enhances thermal performance over time according to the observation given in [14,18]. Since one of the fundamental approaches to improving the stability of nanoPCMEs is to reduce the particle size to the nanoscale specifically below 200 nm, it was performed in this study to improve stability. Smaller particles exhibit increased surface area-to-volume ratios, which enhances their stability against phase separation and thermal cycling effects. Research has shown that nano emulsions with particle sizes in the nanometer range remain stable for extended periods, indicating that size reduction is an effective method for long-term stability [39,40]. The approximate increase rates suggest that the choice of working fluid is crucial for optimizing heat transfer in applications, with nanoPCME_2 combined with iron oxide nanoparticles demonstrating the most promising results. The average Nusselt number enhancement of nanoPCME_2 at 1.1 L/min was obtained by about 25 % as a comparison of pure water. All the nanoPCMEs showed better Nusselt number performance according with the results presented in [41,42] since using iron oxide nanoparticles in nanoPCMEs could provide better overall stability by preventing possible agglomerations between continuous and dispersed phases [43,44].

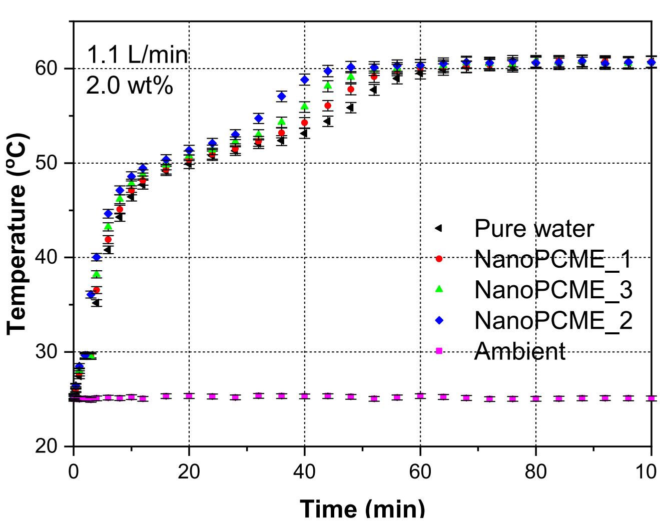

Fig. 11. Wall temperature variations for pure water and different NanoPCMEs.

3.2. *Effects of flow rate, NanoPCME concentration and heat exchanger configuration on energy storage*

The results given in Fig. 13a demonstrate a clear variation between the concentration of nanoPCME_1 and the total energy stored change over time, highlighting the significant impact of nanoparticle concentration on thermal performance. As the concentration increases from 0.5 wt% to 2.0 wt%, there is a marked increase in total enthalpy, with the 2.0 wt% solution achieving nearly over 920 kJ after 12 min, compared to just over 890 kJ for the 0.5 wt% solution. This trend suggests that higher concentrations of nanoPCME_1 enhance the fluid's heat absorption capacity, likely due to improved thermal conductivity and specific heat properties. This provides achieving a steady state faster. Additionally, pure water control exhibits considerably lower total enthalpy, reinforcing the effectiveness of NanoPCME_1 as a thermal enhancement agent. Because the choice of surfactants plays a crucial role in emulsion stability. Surfactants with optimal hydrophilic balance values can effectively stabilize PCM particles in aqueous media therefore, SDS was used in this study to keep nanoPCMEs as stable form [45]. These findings indicate that optimizing the concentration of nanoRT55 could be pivotal for applications requiring efficient heat transfer, such as in cooling systems or thermal management technologies. Fig. 13b demonstrates the variation of energy storage for different nano emulsions over time, revealing that all formulations exhibit an increase in energy stored as they absorb heat. The combinations of iron oxides

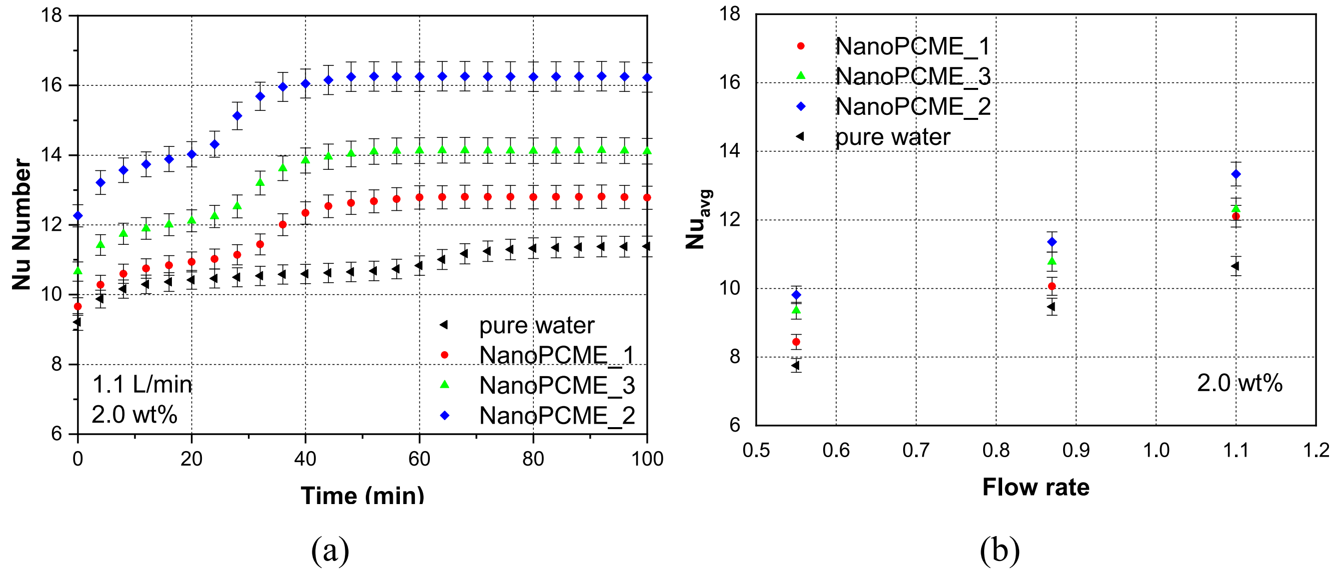

Fig. 12. (a) Nusselt number change of different working fluids for PCM + Metal foam case (b) Average Nusselt number change for different NanoPCMEs

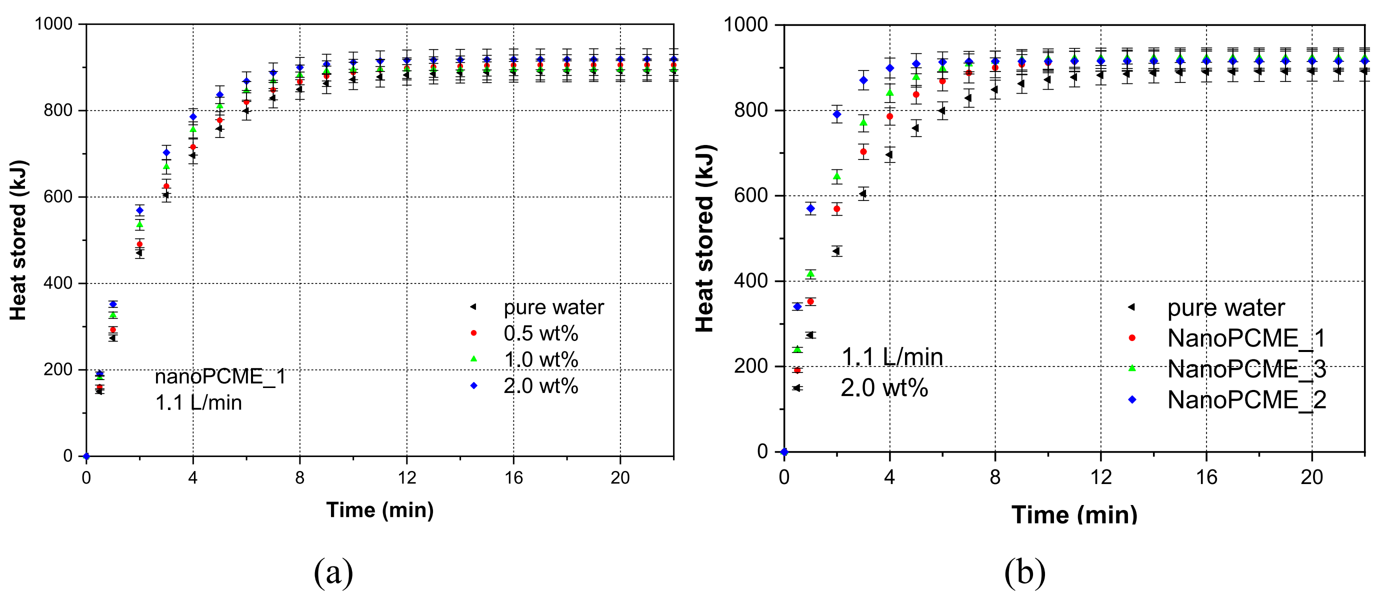

Fig. 13. (a) Total heat storage changes of nanoPCME_1 according to concentration and (b) for different NanoPCMEs.

display significant increases in energy stored, suggesting that these additives enhance the thermal performance of the emulsions. In contrast, pure water demonstrates a markedly lower energy storage increase, emphasizing the effectiveness of nano emulsions in thermal absorption. The curves indicate an asymptotic value, suggesting that the system reaches steady state, with the experiments conducted under consistent conditions (1.1 L/min flow rate and 2.0 wt% concentration) ensuring that the observed variations are attributable to the emulsions themselves. Overall, these findings highlight the potential of nano emulsions for applications in thermal management and energy transfer systems. As can be understood, the total thermal energy storage of the system should be the same for all nanoPCMEs except for duration for reaching the maximum capacity. However, in the experiments there were absolutely heat losses even if the system had good insulation. The reason for the slight differences between each other could be that situation as indicated previously in [7,46].

The total energy stored changes over time for various working fluids under identical conditions (1.1 L/min and 2.0 wt%) are given on Fig. 14. As observed, the enthalpy change varies significantly among the different fluids tested. The curve for NanoRT55 shows a relatively steep increase in energy storage, indicating its effectiveness in heat transfer. In contrast, the mixtures of iron oxides exhibit a more gradual slope, suggesting a slower rate of heat absorption. Pure water, while commonly used as a baseline, demonstrates the least total energy storage change, reinforcing the idea that specialized working fluids can enhance thermal performance.

The data highlights the importance of selecting appropriate working fluids for applications requiring efficient thermal management, as the choice directly influences the system energy efficiency and overall performance. The fastest working fluid reaching the maximum total enthalpy value was the nanoPCME_2 since its thermophysical properties are better than others. Additionally, the maximum storage capacity of heat exchanger with PCM + metal foam is always the same for all working fluid as indicated, but the duration of reaching steady state condition of nanoPCME_2 was around two times faster than pure water.

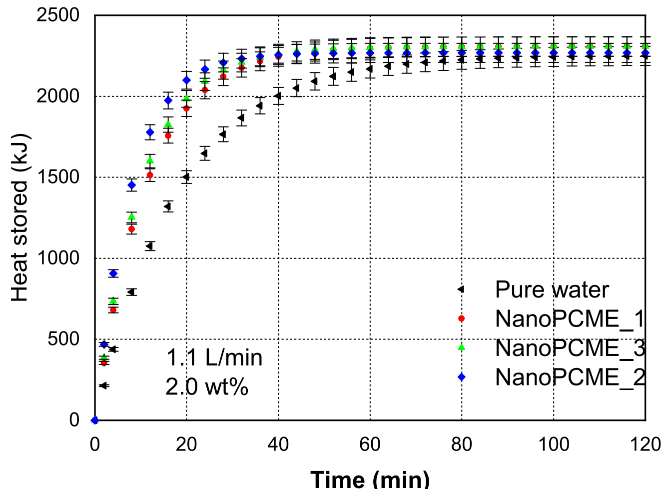

Fig. 14. Total heat storage variation of different working fluids for PCM + metal foam case.

4. Conclusions

The study experimentally investigated the thermal performance of various nanoPCM emulsions as working fluids in heat exchangers, revealing that all tested nanoPCMEs outperformed pure water in convection heat transfer. Two configurations of that heat exchanger were prepared as aluminum solid wall and aluminum profile walls filled with PCM + metal foam. Temperature variation, Nusselt number and thermal energy storage capacities were obtained and compared with each other. Three different nanoPCM emulsions were tested to compare with pure water.

- All nanoPCMEs showed higher convection heat transfer performance than pure water. For the heat exchanger with solid aluminum walls, thermal energy storage was obtained about 900 kJ which is the maximum value of the system. The difference of each working fluid was determined for the duration of reaching maximum stored energy. As a comparison with pure water, 2.0 wt% nanoPCME_2 showed two times faster than pure water to reach maximum stored energy level. On the other hand, this value was calculated for PCM + metal foam heat exchanger 1.6 times faster than pure water since the phase changing process occurred.
- Maximum stored thermal energy with PCM + metal foam configuration was achieved around 2250 kJ due to the high latent heat of PCM layer. As for the Nusselt number, the maximum average Nusselt number was achieved with nanoPCME_2 for all configurations.
- Maximum enhancement of Nusselt number with that working fluid according to pure water was determined as 34.5 % with 2.0 wt% for solid wall heat exchanger. The improvement in Nusselt number with PCM + metal foam heat exchanger was obtained as 41.9 % with 2.0 wt%.
- Highest average *Nu* number has been achieved with nanoPCME_2 with PCM + metal foam case which provided 25 % improvement.
- Overall, the convection heat transfer results of nanoPCMEs were obtained higher than pure water and reached the maximum stored energy as well. These results could be beneficial for any thermal energy storage systems and thermal control systems.

CRediT authorship contribution statement

Hüseyin Kaya: Writing – review & editing, Writing – original draft, Resources, Methodology, Investigation, Formal analysis, Data curation, Conceptualization. **Emre Alp:** Writing – review & editing, Writing – original draft, Methodology, Investigation, Formal analysis, Conceptualization. **Safa Sabet:** Writing – review & editing, Methodology, Formal analysis, Conceptualization. **Bernardo Buonomo:** Writing – review & editing, Resources, Methodology, Formal analysis, Conceptualization. **Laura Fedele:** Writing – review & editing, Methodology, Conceptualization. **Stefano Rossi:** Writing – review & editing, Methodology, Conceptualization. **Oronzio Manca:** Writing – review & editing, Supervision, Conceptualization.

Declaration of competing interest

The authors declare that they have no known competing financial interests or personal relationships that could have appeared to influence the work reported in this paper.

Acknowledgement

This research was partially funded by Bartın University Scientific Research Projects Unit (Project ID number: 2023-FEN-İHP-008), the visiting researcher program of Università degli Studi della Campania “Luigi Vanvitelli” with the grant year 2024 and Università degli Studi della Campania “Luigi Vanvitelli” with the grant “TECSOL” and Ministero dell’Università e della Ricerca with the grant PRIN Bando 2022 PNRR - Prot. P2022NYPHL, Research project title: “VISIONS: eVolutIonary deSign of InnOvative heat traNsfer deviceS” – Funded by European Union – Next Generation EU.

Data availability

Data will be made available on request.

References

[1] O. Mahian, E. Bellos, C.N. Markides, R.A. Taylor, A. Alagumalai, L. Yang, C. Qin, B. J. Lee, G. Ahmadi, M.R. Safaei, S. Wongwises, Recent advances in using nanofluids in renewable energy systems and the environmental implications of their uptake, Nano Energy 86 (2021), https://doi.org/10.1016/j.nanoen.2021.106069.

[2] G. Zhang, M. Wang, X. Yan, G. Cui, B. Dou, W. Lu, Q. Yang, Flow and heat transfer characteristics of microencapsulated phase change material slurry in bonded triangular tubes for thermal energy storage systems, Energy 286 (2024), https://doi.org/10.1016/j.energy.2023.129617.

[3] S. Venkatraman, P. Jidhesh, J.D. Rathnaraj, C. Selvam, Experimental studies on the enhancement in discharging characteristics of phase change material with steatite nanoparticles, J Energy Storage 73 (2023), https://doi.org/10.1016/j.est.2023.109103.

[4] K. Chandra, S. Sabet, H. Kaya, B. Buonomo, O. Manca, A transient numerical approach for phase change material effect on mixed convection in an open cavity, Int. Commun. Heat Mass Transf. 148 (2023), https://doi.org/10.1016/j.icheatmasstransfer.2023.107051.

[5] A.M. Bassam, K. Sopian, A. Ibrahim, M.F. Fauzan, A.B. Al-Aasam, G.Y. Abusaibaa, Experimental analysis for the photovoltaic thermal collector (PVT) with nano PCM and micro-fins tube nanofluid, Case Stud. Therm. Eng. 41 (2023) 102579, https://doi.org/10.1016/j.csite.2022.102579.

[6] M. Joseph, V. Sajith, An investigation on heat transfer performance of polystyrene encapsulated n-octadecane based nanofluid in square channel, Appl. Therm. Eng. 147 (2019) 756–769, https://doi.org/10.1016/j.applthermaleng.2018.10.120.

[7] J. Zhang, G. Zhang, G. Cui, B. Dou, X. Yan, W. Lu, Q. Yang, Experimental investigation of the effects of metal oxides and nucleating agents on nano-emulsions heat transfer performance in mini-channels, Appl. Therm. Eng. 226 (2023), https://doi.org/10.1016/j.applthermaleng.2023.120312.

[8] C.J. Ho, S.T. Hsu, J.H. Jang, S.F. Hosseini, W.M. Yan, Experimental study on thermal performance of water-based nano-PCM emulsion flow in multichannel heat sinks with parallel and divergent rectangular mini-channels, Int. J. Heat Mass Transf. 146 (2020), https://doi.org/10.1016/j.ijheatmasstransfer.2019.118861.

[9] R. Hidki, L. El Moutaouakil, M. Boukendil, Z. Charqui, Z. Zrikem, A. Abdelbaki, Natural convection heat transfer analysis of a nano-encapsulated phase change material (NEPCM) confined in a porous square chamber with two heat sources, J Energy Storage 73 (2023), https://doi.org/10.1016/j.est.2023.108924.

[10] G. Zhang, Y. Guo, B. Zhang, X. Yan, W. Lu, G. Cui, Y. Du, Preparation and control mechanism of nano-phase change emulsion with high thermal conductivity and low supercooling for thermal energy storage, Energy Rep. 8 (2022) 8301–8311, https://doi.org/10.1016/j.egyr.2022.06.029.

[11] D. Cabaleiro, F. Agresti, L. Fedele, S. Barison, C. Hermida-Merino, S. Losada-Barreiro, S. Bobbo, M.M. Piñeiro, Review on phase change material emulsions for advanced thermal management: design, characterization and thermal performance, Renew. Sust. Energ. Rev. 159 (2022), https://doi.org/10.1016/j.rser.2022.112238.

[12] E. Golab, S. Goudarzi, H. Kazemi-Varnamkhasti, H. Amigh, F. Ghaemi, D. Baleanu, A. Karimipour, Investigation of the effect of adding nano-encapsulated phase change material to water in natural convection inside a rectangular cavity, J Energy Storage 40 (2021), https://doi.org/10.1016/j.est.2021.102699.
[13] H.R. Seyf, M.R. Wilson, Y. Zhang, H.B. Ma, Flow and heat transfer of nanoencapsulated phase change material slurry past a unconfined square cylinder, J. Heat Transf. 136 (2014), https://doi.org/10.1115/1.4025903.
[14] S.K. Singh, S.K. Verma, R. Kumar, Thermal performance and behavior analysis of SiO2, Al2O3 and MgO based nano-enhanced phase-changing materials, latent heat thermal energy storage system, J Energy Storage 48 (2022) 103977, https://doi.org/10.1016/j.est.2022.103977.
[15] B. Kok, Examining effects of special heat transfer fins designed for the melting process of PCM and Nano-PCM, Appl. Therm. Eng. 170 (2020), https://doi.org/10.1016/j.applthermaleng.2020.114989.
[16] C.R.E.S. Nóbrega, K.A.R. Ismail, F.A.M. Lino, Thermal performance of bare and finned tubes submersed in nano-PCM mixture, J. Braz. Soc. Mech. Sci. Eng. 43 (2021) 1–14, https://doi.org/10.1007/s40430-020-02740-5.
[17] A.E. Kabeel, R. Sathyamurthy, A.M. Manokar, S.W. Sharshir, F.A. Essa, A. H. Elshiekh, Experimental study on tubular solar still using graphene oxide Nano particles in phase change material (NPCM'S) for fresh water production, J Energy Storage 28 (2020), https://doi.org/10.1016/j.est.2020.101204.
[18] A. Sathishkumar, M. Cheralathan, Charging and discharging processes of low capacity nano-PCM based cool thermal energy storage system: an experimental study, Energy 263 (2023), https://doi.org/10.1016/j.energy.2022.125700.
[19] V.P. Kalbande, G. Fating, M. Mohan, K. Rambhad, A.K. Sinha, Experimental and theoretical study for suitability of hybrid nano enhanced phase change material for thermal energy storage applications, J Energy Storage 51 (2022), https://doi.org/10.1016/j.est.2022.104431.
[20] R. Yadollahi Farsani, A. Raisi, A. Mahmoudi, Successive melting and solidification of paraffin–alumina nanomaterial in a cavity as a latent heat thermal energy storage, J. Braz. Soc. Mech. Sci. Eng. 41 (2019) 1–14, https://doi.org/10.1007/s40430-019-1859-8.
[21] L. Liu, J. Niu, J. Wu, Preparation of stable phase change material emulsions for thermal energy storage and thermal management applications: a review, Materials (Basel) 15 (2022).
[22] J. Zhou, J. Zhao, H. Li, Y. Cui, X. Li, Enhanced thermal properties for nanoencapsulated phase change materials with functionalized graphene oxide (FGO) modified PMMA, Nanotechnology 31 (2020), https://doi.org/10.1088/1361-6528/ab898b.
[23] T.D. Gamot, A.R. Bhattacharyya, T. Sridhar, A.J. Fulcher, F. Beach, R.F. Tabor, M. Majumder, Enhanced thermal conductivity of high internal phase emulsions with ultra-low volume fraction of graphene oxide, Langmuir 35 (2019) 2738–2746, https://doi.org/10.1021/acs.langmuir.8b04116.
[24] H. Mhiri, A. Jemni, H. Sammouda, Thermal behavior of CompositeMaterial (nanoPCM/aluminumfoam) used for thermal energy storage (TES) applications, Comptes Rendus Phys. 21 (2020) 233–252, https://doi.org/10.5802/CRPHYS.2.
[25] H. Liu, X. Wang, D. Wu, Innovative design of microencapsulated phase change materials for thermal energy storage and versatile applications: a review, sustain, Energy Fuel 3 (2019) 1091–1149, https://doi.org/10.1039/c9se00019d.
[26] Q. Zhang, Y. Shi, Z. Tu, Y. Hu, C. He, Emulsion properties during microencapsulation of Cannabis oil based on protein and sucrose esters as emulsifiers: stability and rheological behavior, Foods 11 (2022), https://doi.org/10.3390/foods11233923.
[27] Y. He, F. Wu, X. Sun, R. Li, Y. Guo, C. Li, L. Zhang, F. Xing, W. Wang, J. Gao, Factors that affect Pickering emulsions stabilized by graphene oxide, ACS Appl. Mater. Interfaces 5 (2013) 4843–4855, https://doi.org/10.1021/am400582n.
[28] A. Pal, R. Pal, Rheology of emulsions thickened by starch nanoparticles, Nanomaterials 12 (2022) 1–20, https://doi.org/10.3390/nano12142391.
[29] R. Cao, Y. Wang, S. Chen, N. Han, H. Liu, X. Zhang, Multiresponsive shape-stabilized Hexadecyl acrylate-grafted graphene as a phase change material with enhanced thermal and electrical conductivities, ACS Appl. Mater. Interfaces 11 (2019) 8982–8991, https://doi.org/10.1021/acsami.8b18282.
[30] Y. Wang, Z. Chen, X. Ling, An experimental study of the latent functionally thermal fluid with micro-encapsulated phase change material particles flowing in microchannels, Appl. Therm. Eng. 105 (2016) 209–216, https://doi.org/10.1016/j.applthermaleng.2016.05.159.
[31] P. Hu, L. Kang, T. Chang, F. Yang, H. Wang, Y. Zhang, J. Yang, K. She Wang, J. Du, Z. Yang, High saturation magnetization Fe3O4 nanoparticles prepared by one-step reduction method in autoclave, J. Alloys Compd. 728 (2017) 88–92, https://doi.org/10.1016/j.jallcom.2017.08.290.
[32] S.S. Shijina, S. Akbar, V. Sajith, Graphene functionalized nano-encapsulated composite phase change material based nanofluid for battery cooling: an experimental investigation, Appl. Therm. Eng. 259 (2025), https://doi.org/10.1016/j.applthermaleng.2024.124893.
[33] L. Colla, L. Fedele, S. Mancin, L. Danza, O. Manca, Nano-PCMs for enhanced energy storage and passive cooling applications, Appl. Therm. Eng. 110 (2017) 584–589, https://doi.org/10.1016/j.applthermaleng.2016.03.161.
[34] Rubitherm, Data Sheet of RT55. https://www.rubitherm.eu/media/products/datasheets/Techdata_-RT55_EN_09102020.PDF, 2025.
[35] F.P. Incropera, T.L. Bergman, A.S. Lavine, D.P. DeWitt, Fundamentals of Heat and Mass Transfer, 7th ed., John Wiley & Sons, Haboken, New Jersey, 2011.
[36] R.J. Moffat, Describing the uncertainties in experimental results, Exp. Thermal Fluid Sci. 1 (1988) 3–17, https://doi.org/10.1016/0894-1777(88)90043-X.
[37] N.H. Khairul Anuar, M.N. Mhd Razali, M.R. Mohamad Yasin, M. Abdul Hadi, A. N. Abd, Ghaffar, Study on custom centrifugal pump performance in supplying food based high viscos liquid, J. Mod. Manuf. Syst. Technol. 5 (2021) 80–88, https://doi.org/10.15282/jmmst.v5i1.6280.
[38] V. Soni, S. Saber, H. McPhee, J. Riordon, M. Zargartalebi, M. Holmes, M. Toews, D. Sinton, Evaluation of a microencapsulated phase change slurry for subsurface energy recovery, Energy Fuel 35 (2021) 10293–10302, https://doi.org/10.1021/acs.energyfuels.1c00972.
[39] L. Liu, J. Niu, J.Y. Wu, Formulation of highly stable PCM nano-emulsions with reduced supercooling for thermal energy storage using surfactant mixtures, Sol. Energy Mater. Sol. Cells 223 (2021) 110983, https://doi.org/10.1016/j.solmat.2021.110983.
[40] P. Schalbart, M. Kawaji, K. Fumoto, Formation of tetradecane nanoemulsion by low-energy emulsification methods, Int. J. Refrig. 33 (2010) 1612–1624, https://doi.org/10.1016/j.ijrefrig.2010.09.002.
[41] G. Murali, P. Ramani, M. Murugan, P.V. Elumalai, N.U. Ranjan Goud, S. Prabhakar, Improved solar still productivity using PCM and nano- PCM composites integerated energy storage, Sci. Rep. 14 (2024) 1–12, https://doi.org/10.1038/s41598-024-65418-1.
[42] L. Zhang, H. Kazemi-Varnamkhasti, A. Basem, H. Hamza, A.J. Sultan, M. Al-Bahrani, C. Padilla, S.B. Formanova, S. Salahshour, A. Alizadeh, Improving the thermal performance of nano-encapsulated phase change material slurry by changing fins configurations in a rectangular cavity, Int. Commun. Heat Mass Transf. 157 (2024), https://doi.org/10.1016/j.icheatmasstransfer.2024.107739.
[43] S. Bom, M. Fitas, A.M. Martins, P. Pinto, H.M. Ribeiro, J. Marto, Replacing synthetic ingredients by sustainable natural alternatives: a case study using topical O/W emulsions, Molecules 25 (2020), https://doi.org/10.3390/MOLECULES25214887.
[44] M. Noshad, M. Mohebbi, A. Koocheki, F. Shahidi, Influence of interfacial engineering on stability of emulsions stabilized with soy protein isolate, J. Dispers. Sci. Technol. 37 (2016) 56–65, https://doi.org/10.1080/01932691.2015.1027907.
[45] M. Shayanmehr, F. Eslami, Stability of n-hexadecane phase change material emulsions using sugar-based surfactants and the HLD platform, J. Surfactant Deterg. 27 (2024) 567–579, https://doi.org/10.1002/jsde.12745.
[46] T. Morimoto, H. Kumano, Natural convection characteristics of phase-change material emulsions in a rectangular vessel with vertical heating/cooling walls, Int. J. Heat Mass Transf. 183 (2022), https://doi.org/10.1016/j.ijheatmasstransfer.2021.122234.